Comparative evaluation of creep response of X20 and P91 steam piping networks in operation

Smith Salifu[a*], Dawood Desai[a], Schalk Kok[b]

[a] Department of Mechanical and Automation Engineering, Tshwane University of Technology, Pretoria, South Africa

[b] Department of Mechanical and Aeronautical Engineering, University of Pretoria, Pretoria, South Africa

Corresponding author[*]: smithsalifu@gmail.com

Abstract

The geometrical increase in the demand for electrical energy has posed serious pressure on the power generation components such as the steam pipes due to the consequential increase in the operating parameters such as temperature and pressure. This increment in operating parameters tends to limit the useful life of these pipes. Thus, high creep resistant materials such as X20 CrMoV12-1 and P91 (9Cr-1Mo) are used to manufacture steam pipes. In this paper, the creep behaviour of X20 CrMoV12-1 and P91 (9Cr-1Mo) steam piping network subjected to typical operating condition was determined via a finite element analysis code, Abaqus CAE/2017 alongside fe-safe/Turbolife software, and their results were compared. The maximum creep stress, strain rate, creep damage and worst creep life in both piping materials were developed on the intrados of the elbow, with P91 steam pipe having higher useful creep life. Furthermore, a good correlation was achieved between the result of the analytically calculated and numerically simulated creep rate at the straight section of the piping networks.

Keywords: Creep rate, creep damage, creep life, intrados, subroutine, piping network

Introduction

The quest to create a balance between the ever-growing demand for electrical energy and its supply has resulted in the constant increase of the power plant's operating parameters like the pressure and temperature. In order to meet up with this demand, the steam pipes, which is one of the important components of power plants, must possess unique material properties capable of withstanding the harsh operating conditions it will be subjected to. Hence, steam pipes are made from martensitic steels like X20 CrMoV12-1 (ferritic stainless steel containing 12% chromium) and P91 (9Cr-1Mo) [1] due to their higher creep strength, good corrosion resistance [2] and fantastic weldability property [3,4,5] displayed by both steels at high temperature. Both steels are often used in steam generator as headers and also as tubing for conveying steam from the boiler to the turbine compartment. The high strength displayed by the steels at elevated temperature can be attributed to their complex microstructures, which exhibit high dislocation density consisting of lath and subboundaries that show MX and M23C6 type precipitates in the matrix [5]. Also, the very minute MX type inter-particle precipitates in addition to the increased volume fraction and resistance to coarsening account for the improved creep strength of the steel [5].

Several challenges are involved during creep damage modelling, and these challenges have been widely explored in the literature [6, 7]. It was discovered that there is severe difficulty in creep cavity quantification and characterization, and the development of damage criterion for materials. Furthermore, the development and application of novel creep model and formulation capable of handling a wide range of stress was another challenge encountered.

Since the creep rate of components during operation strongly depends on temperature and pressure, several creep equations and models have been proposed. Some of these creep models/equations show

the relationship between the steady-state creep strain rate under hot deformation conditions or creep condition when the component is subjected to stress either in tension and in compression [8]. Hence, under creep conditions, a new generation expression termed the modified hyperbolic sine creep law that possesses the exceptional ability to effectively account for both high and low-stress range was proposed by Garofalos [9], and under hot deformation, the same model was proposed by Sellars and Tegart [8].

The service life prediction of steam pipes under creep condition is of keen interest to power plant operators since the steam pipes operate at elevated temperatures. For engineering components such as pipes and pipe related components [10,11,12,13,14], the use of damage continuum mechanics in conjunction with finite element (FEA) technique becomes very useful for the prediction of their useful creep life [11, 15]. The continuum damage mechanic model is based on the concepts of Kachanov [11, 16], and it attempts to characterize the full creep behaviour of components in creep environment. Other frequently used creep models include one-state variable constitutive equation and multi-state variables constitutive equation that represent the creep deformation and failure mechanisms of components [17].

Over time, the simplicity of the power-law creep model makes it attractive for computing creep rate, but both the strain-hardening and time-hardening version of law are limited by relatively low stress state and constants when applied [18]. Since the stress around the tips of cracks are relatively high and creep strain rates are exponentially dependent on stress at high stresses, hyperbolic sine creep model well known for its exponential dependence on stress at high-stress levels [18], and ability to take into account high and low-stress range [8] should be implored when determining the creep rate and behaviour of components in creep environment.

In this study, the creep behaviour of two frequently used steam piping materials, X20 and P91 steel pipes, under typical operation conditions was computed via finite element analysis code, Abaqus CAE/2017. The phenomenological modified hyperbolic sine creep model user subroutine script used was written in Fortran and implemented in Abaqus, while the useful remaining creep life and damage of the piping network was computed using fe-safe/Turbolife software.

Thermo-mechanical stress in a thick pipe

When thick cylinder or pipe is subjected to internal pressure, radial stress σ_r, circumferential stress, σ_t and axial or longitudinal stress, σ_z are the three stresses developed. The pressure force on the head of the pipe accounts for the constant longitudinal stress developed in the pipe, while the radial and circumferential stresses developed are known to vary throughout the pipe [19]. If a thick cylinder or straight pipe with an internal and external radius r_i and r_o respectively is acted upon by internal pressure of magnitude P, Lamé [20] introduced the generalized expression for the three forms of stresses that are developed in the pipe as shown below:

$$\sigma_r = P\frac{r_i^2(r^2-r_o^2)}{r^2(r_o^2-r_i^2)} \quad (1)$$

$$\sigma_t = P\frac{r_i^2(r^2+r_o^2)}{r^2(r_o^2-r_i^2)} \quad (2)$$

$$\sigma_z = \frac{P_i r_i^2}{r_o^2-r_i^2} \quad (3)$$

Also, the effective mechanical stress of the straight pipe can be determined using the von-Mises theory.

$$\sigma_m = \sqrt{[\sigma_t^2 + \sigma_r^2 + \sigma_z^2 - (\sigma_t\sigma_r + \sigma_t\sigma_z + \sigma_r\sigma_z)]} \quad (4)$$

where σ_m represent the effective or total Von-Mises stress developed in the pipe.

Similarly, the developed thermal stress in thick straight pipe [21, 22] with internal radius, r_i, and external radius, r_o, is given by

$$\sigma_{tT} = \frac{\alpha E}{(1-v)r^2}\left[\frac{r^2+r_i^2}{r_o^2-r_i^2}\int_{r_i}^{r_o} Trdr - \int_{r_i}^{r} Trdr - Tr^2\right] \quad (5)$$

$$\sigma_{rT} = \frac{\alpha E}{(1-v)r^2}\left[\frac{r^2-r_i^2}{r_o^2-r_i^2}\int_{r_i}^{r_o} Trdr - \int_{r_i}^{r} Trdr\right] \quad (6)$$

$$\sigma_{zT} = \frac{\alpha E}{(1-v)}\left[\frac{2}{r_o^2-r_i^2}\int_{r_i}^{r_o} Trdr - T\right] \quad (7)$$

The effective thermal stress is determined using von-Mises theory.

$$\sigma_T = \sqrt{[\sigma_t^2 + \sigma_r^2 + \sigma_z^2 - (\sigma_t\sigma_r + \sigma_t\sigma_z + \sigma_r\sigma_z)]} \quad (8)$$

where σ_r represents the radial mechanical stress, σ_t represents the circumferential mechanical stress and σ_z represents the axial mechanical stress. σ_{rT} represents the thermal radial stress, σ_{tT} represents thermal circumferential stress and σ_{zT} represents axial thermal stress. σ_m and σ_T represent the effective or total von-Mises mechanical stress and thermal stress respectively.

Hence, the developed effective thermo-mechanical stress, σ_{TM}, in a straight thick pipe is obtained by the summation the two effective von-Mises stresses obtained.

$$\sigma_{TM} = \sigma_m + \sigma_T \quad (9)$$

Creep model

For components in service under creep environment, creep strain rate expression capable of adequately accounting for the creep strain rate over a vast stress range was proposed by Garofalo [8, 9]. A similar expression was proposed by Sellars and Tegar for components subjected to hot deformation [8]. The proposed creep model is known to effectively describe the relationship that exists between the temperature of deformation, flow stress and creep strain rate. The expression for the modified hyperbolic sine creep model that is capable of accounting for the different regime of stresses is given as

$$\dot{\varepsilon}_{cr} = A(\sinh[\sigma H]^n)\exp\left(\frac{-Q}{RT}\right) \quad (10)$$

where H, n and A are material constants; Q represents the activation energy (J/(molK); T represents the operating temperature in kelvin (K) and the gas constant is represented with R (J/(molK).

Damage model

Ductility exhaustion theory presumes that a critical ductility characterized by the induction of forward crack propagation is developed when a component experiences local strain [23, 24]. Hence, at failure, the creep strain rate to creep strain ratio can be used to determine the creep strain damage as depicted in Eq. (11).

$$d_c = \frac{\varepsilon_c}{\varepsilon_f^*} \tag{11}$$

where d_c is the creep damage, ε_c represents the creep strain rate and ε_f^* represents multiaxial creep strain at failure strain.

Due to the complexity in the nature of the creep strain developed at intricate parts such as that obtained at the elbows of a piping network, the value of ε_f^* obtained is quite different from that obtained in uniaxial creep strain, ε_f. Thus, it is paramount to create a proper relationship between both strains to accurately determine the creep damage. In view of this, many multiaxial creep ductility factors (MCDF) that shows the ratio of multiaxial creep strain to uniaxial creep strain at failure have been proposed. Wen [25] proposed MCDF that is based on the theory of coalescence and cavity growth defined as

$$\frac{\varepsilon_f^*}{\varepsilon_f} = \exp\left[\frac{2}{3}\left(\frac{n-0.5}{n+0.5}\right)\right] / \exp\left[2\left(\frac{n-0.5}{n+0.5}\right)\frac{\sigma_m}{\sigma_e}\right] \tag{12}$$

where σ_m and n is hydrostatic stress and material constant respectively.

This model proffers a higher multiaxial creep strain accuracy when compared with other MCDFs [25].

When a material defined as a function temperature and stress displays limiting creep life before rupture, the cumulative damage is presumed to occur without the influence of the order in which the stress was applied. Hence, the linear damage rule proposed by Robinson is deemed suitable for such materials [26, 27]. The creep linear damage rule is given as

$$D_c = \sum \frac{t_i}{T_r} \tag{13}$$

where D_c represents creep damage, t_i represents the duration of creep at the operating stress and temperature, and T_r represents creep life before rupture.

Model verification

Using Abaqus CAE/2017 software, the FEA model for the heat transfer and creep analysis was developed, while the useful/worst creep life and damage of the piping network were determined with fe-safe/Turbolife software by postprocessing the output database (.odb) results obtained from the conducted creep analysis. The phenomenological modified hyperbolic sine creep model script was written in Fortran and used via a user-subroutine procedure in the Abaqus.

FE model

3D model of power generation pipe-insulation jacket was developed in Abaqus to capture and compare the precise creep behaviour of the steam piping network made of X20 and P91 steel subjected to a real service condition. The part model of the steel piping, insulation jacket, and the pipe-insulation assembly is depicted in Figs. 1, 2, and 3.

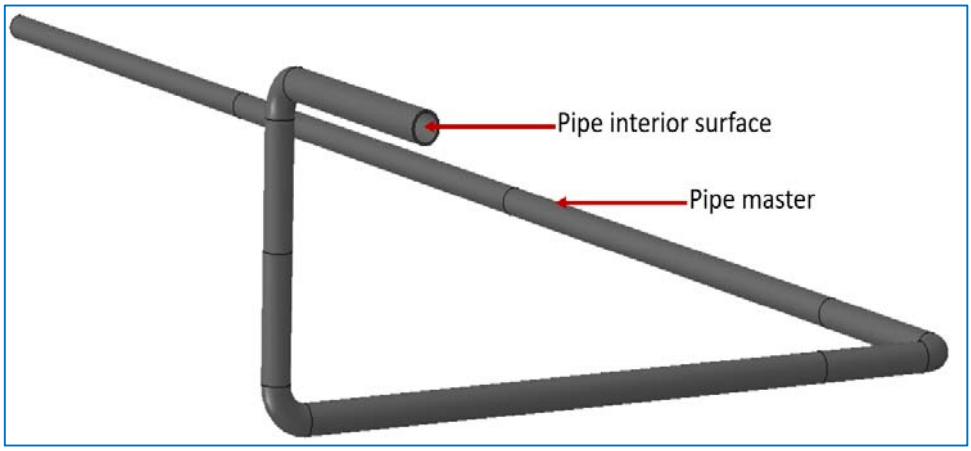

Fig. 1. Model of piping

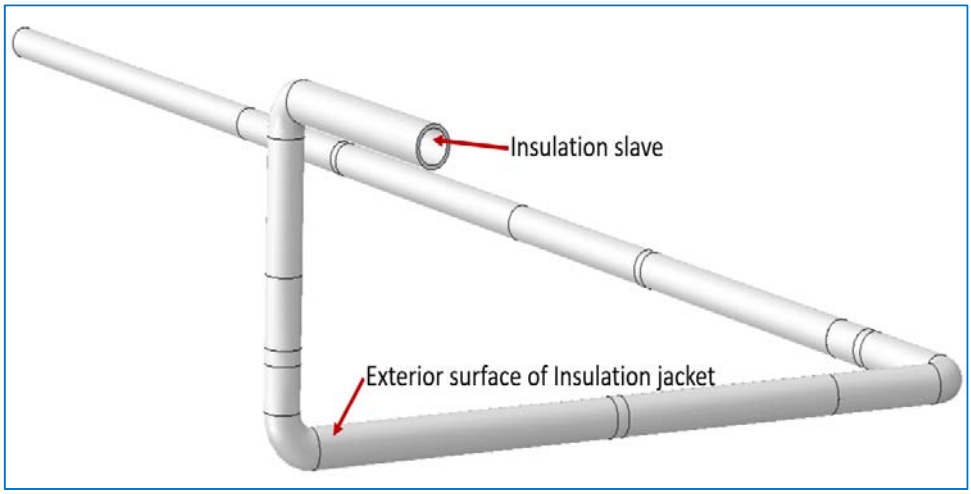

Fig. 2. Model of insulation jacket

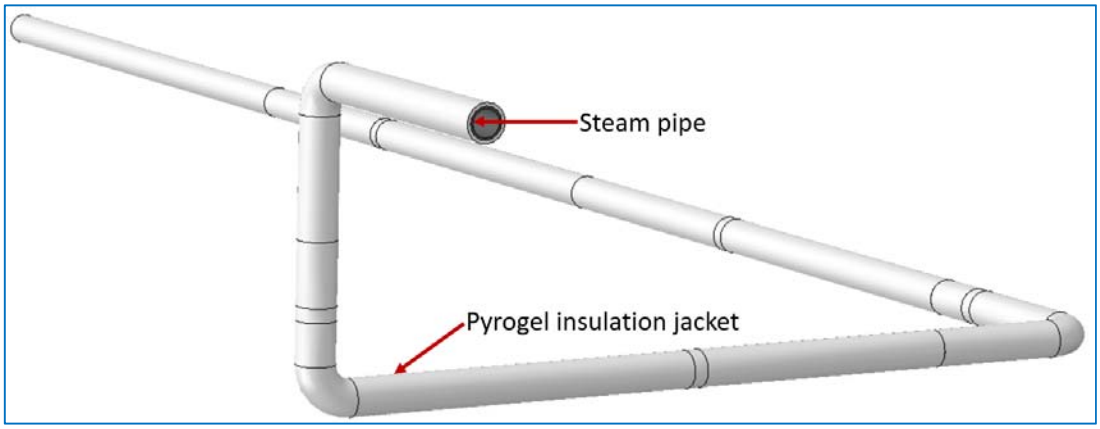

Fig. 3. Model of pipe-insulation jacket

Tables 1 and 2 show the dimensions of the X20 steel piping and insulation jacket (pyrogel) used in this study, while their material properties are depicted in Tables 3 and 4 respectively. Also shown in Figs. 5, 6, and 7 is the temperature-dependent material properties of P91 steel pipe used in this analysis. The analysis was conducted sequentially starting with the thermal/heat transfer analysis [35,

36] due to the influence of temperature on the stress developed during creep analysis but not vice versa [36].

Table 1 Steel pipe dimension [28, 29]

Total pipe length (m)	Pipe diameter		Pipe thickness (m)	Radius of elbow (m)
	External (m)	Internal (m)		
52.10	0.44	0.38	0.03	0.50

Table 2 Pyrogel insulation jacket dimensions [30,31,32]

Total insulation length(m)	Insulation diameter		Insulation thickness(m)	Radius of elbow (m)
	External(m)	Internal(m)		
52.10	0.54	0.44	0.05	0.50

Table 3 X20 steel material constant [33]

Elasticity(GPa)	Poisson ratio	Conductivity (W/mK)	Expansion ($\times 10^{-6}$ K^{-1})	Specific heat capacity(J/kgK)	Density (kg m^{-3})
200.0	0.28	28.0	10.0	460.0	7800.0

Table 4 Pyrogel insulation jacket material constant [31, 34]

Elasticity (MPa)	Poisson ratio	Conductivity ($\times 10^{-6}$ W/mK)	Expansion ($\times 10^{-7}$ K^{-1})	Density (kg m^{-3})	Specific heat capacity (J/kgK)
10.0	0.20	64.0	40.0	171.0	2300.0

Mesh convergence study conducted using the thermomechanical stress developed during the analysis shows that 50-mm seed size having 92196 DC3D8 element type was suitable for the heat transfer analysis, while 50-mm seed size having 92196 C3D8R element type was suitable for the creep analysis. Sink temperature load of 550 °C representing the operating temperature of steam with 10,000 W/m^2K film coefficient was applied to the inner surface of the piping, while a 25 °C sink temperature having 18 W/m^2K heat transfer coefficient was applied to the outer surface of the assembly [31, 32, 37]. Also, 18-MPa pressure load depicting the operating pressure of steam pipe was applied to the inner surface of the piping network, while an appropriate boundary condition that mimics the real case scenario was applied to the assembly. The displacement/rotation mechanical boundary condition was applied in such a way that the assembly is allowed displacement in the x, y and z directions and rotate at the elbow in the x_{R1}, y_{R2} and z_{R3} directions as depicted in Fig. 4.

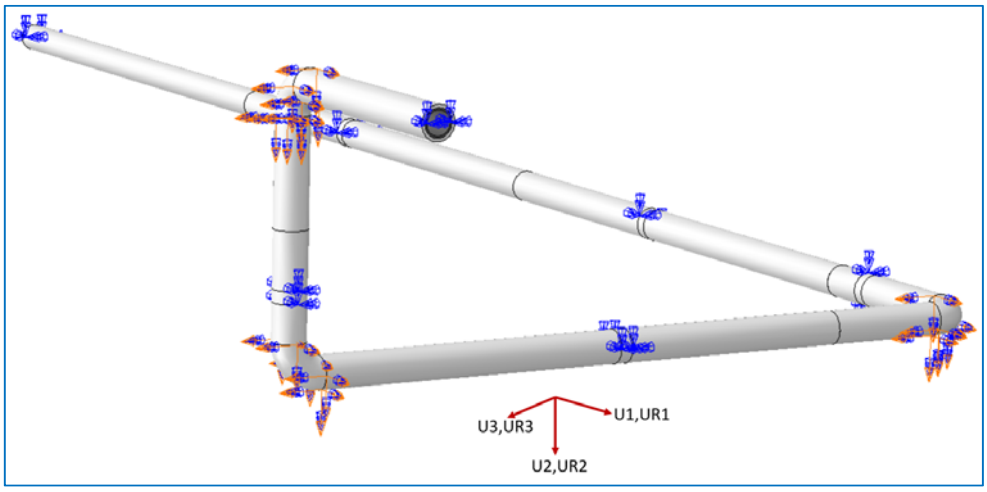

Fig. 4. Boundary conditions applied on assembly model

Creep parameters and damage model

Thermal, elastic/plastic material properties (Figs. 5, 6, and 7; Table 3) and the modified hyperbolic sine creep model constants of X20 and P91 steel obtained via curve fitting of the creep data of X20

[38] and P91 [39] at 550 °C was implemented into the finite element model. The Poisson's ratio and thermal conductivity of P91 steel used is 0.33 and 33 W/mK respectively. Also, through a creep user-subroutine procedure, the Fortran script for the creep model was implemented and executed in Abaqus. Tables 5 and 6 show the creep constants of the two piping materials obtained through curve fitting.

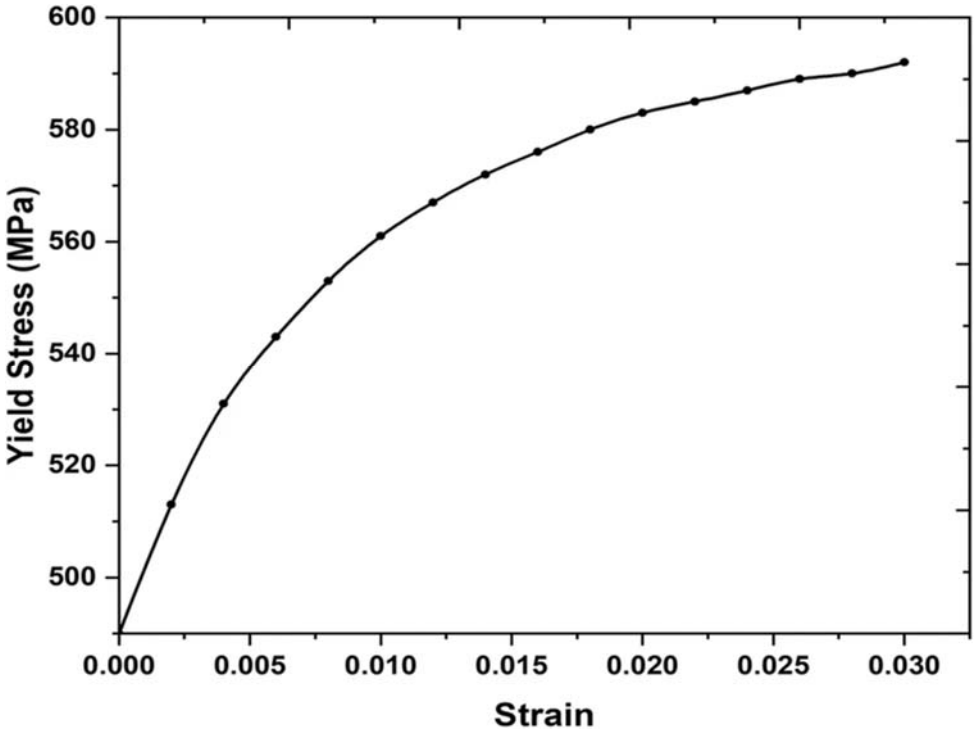

Fig. 5. Plasticity of P91 steel [29]

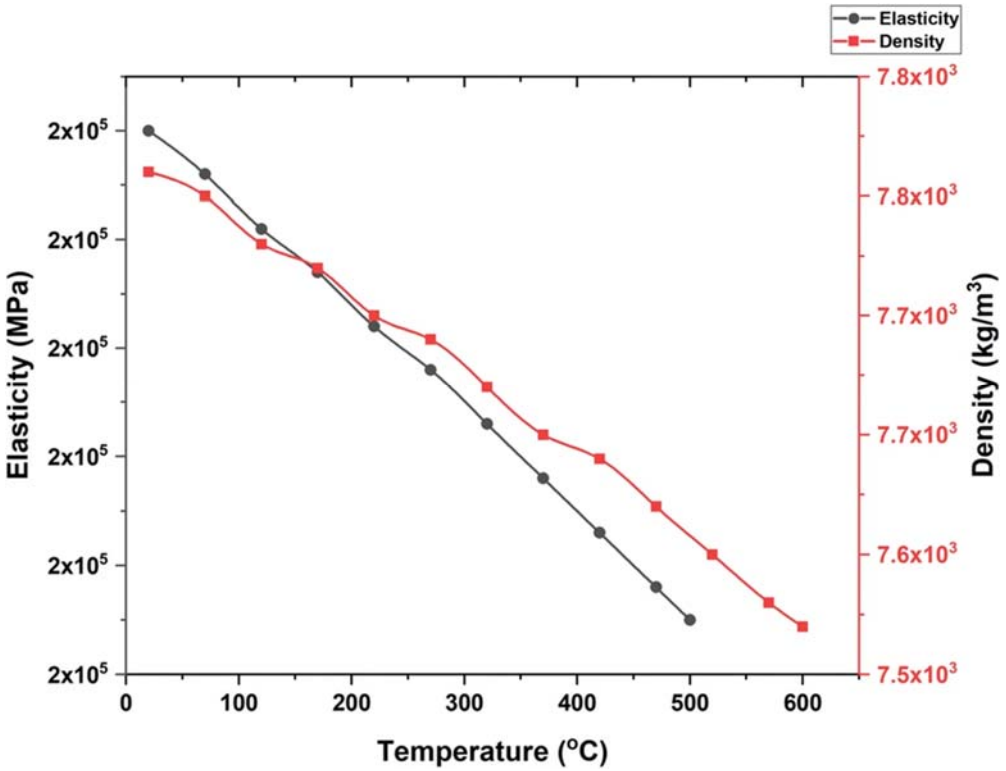

Fig. 6. Temperature-dependent elasticity density of P91 steel [29]

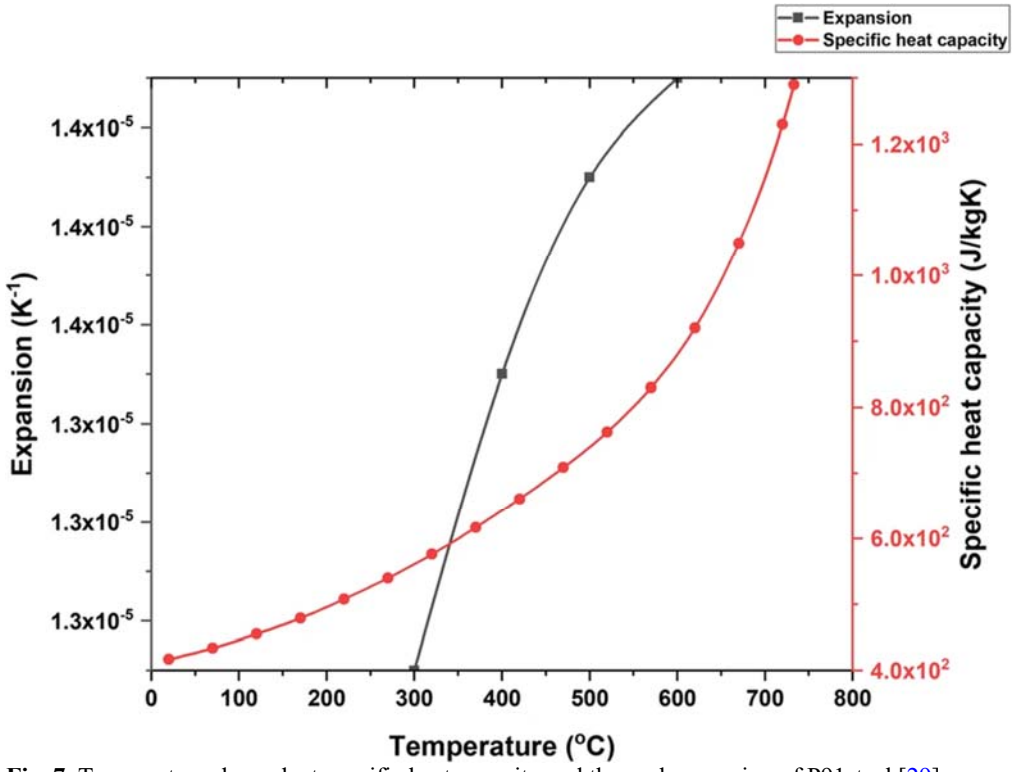

Fig. 7. Temperature-dependent specific heat capacity and thermal expansion of P91steel [29]

Table 5 X20 steel creep material constants at 550 °C [38]

A (× 10^{22} h^{-1})	H (× 10^{-8} Pa)	n	Q (J/(molK))	T (K)	R (J/mol)
10.59	24.90	0.672	530,811.1	823	8.314

Table 6 P91 steel creep material constants at 550 °C [39]

A ($\times 10^{28}$ h^{-1})	H ($\times 10^{-9}$ Pa)	n	Q (J/(molK))	T (K)	R (J/mol)
35.0	23.7	1.32	599,342.4	823	8.314

The damage and useful creep life of the two piping network were obtained using fe-safe/Turbolife software. Turbolife properties were activated, and the Neuber plasticity technique having 0.3 follow-up factor was used. Also, the ductility exhaustion method with Morrow correction algorithm [40] was applied. Furthermore, two surface finishes namely machined-finish surface with $16 < Ra \leq 40$ μm and fine machined-finish surface with $4 < Ra \leq 16$ μm were used in this analysis.

Result and Discussion

In the analysis, a 50-mm mesh size having 92126 elements and 155162 nodes was discovered suitable after the mesh convergence study conducted. Depicted in Fig. 8 is the graph of the mesh convergence study conducted, while Fig. 9 shows the meshed assembly model.

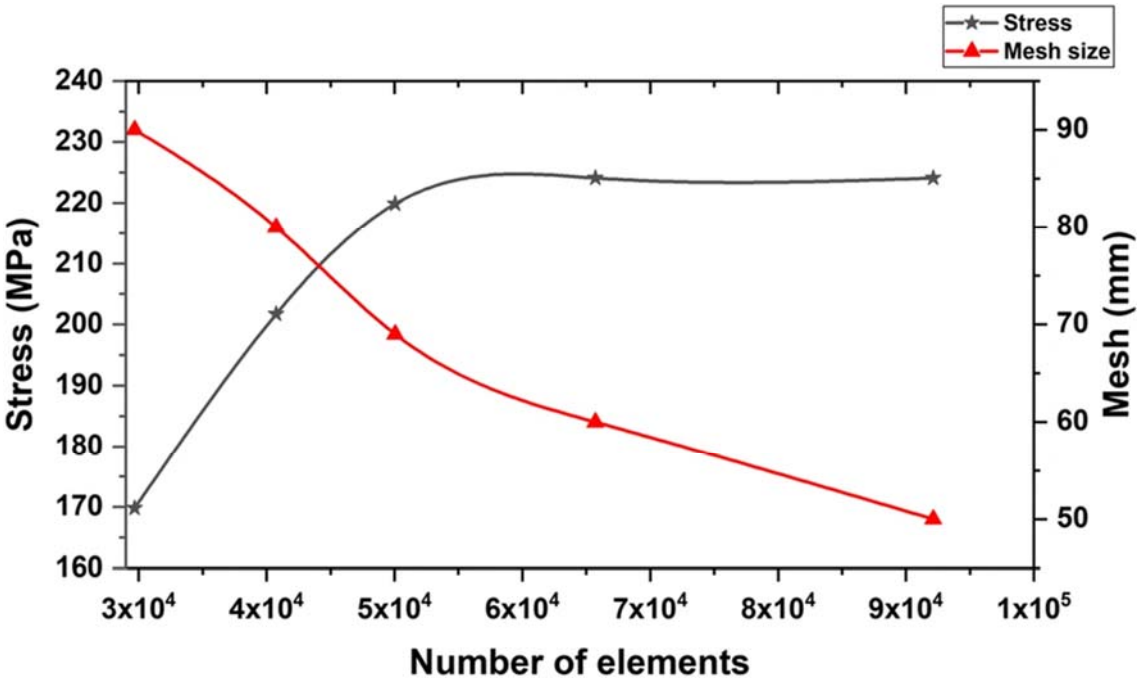

Fig. 8. Graph for mesh convergence study

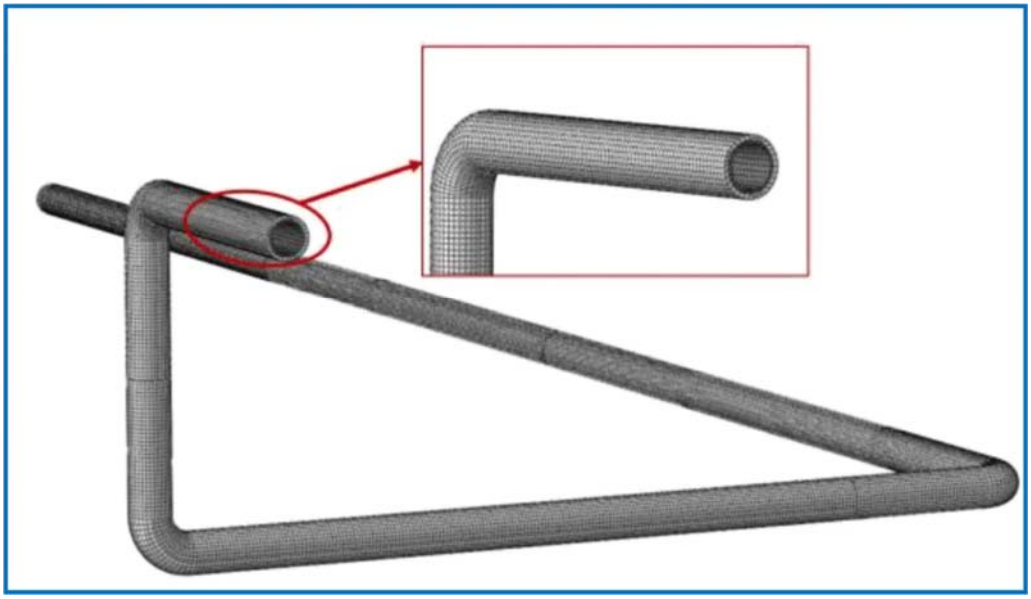

Fig. 9. Assembly mesh for pipe-insulation jacket

Displayed in Fig. 10 a and b is the plot (contour) and temperature distribution attained during heat transfer analysis of X20 and P91 steam piping respectively. From the plot, it was obvious that the optimum operating temperature was used to drive the analysis in both pipes. However, the temperature was observed to drop across the wall thickness of the assembly such that the minimum temperature on the X20 pipe-insulation assembly dropped to the lowest value of 39.9 °C and that on the P91 pipe insulation assembly dropped to 42.9 °C. The difference in the minimum temperature on the insulation jackets can be ascribed to the difference in heat conductivity of the two piping materials. The minute value of temperature on both insulation jackets as compared with the operating temperature is a pointer to the fact that pyrogel can be considered as a good insulation jacket suitable for insulating high-temperature components and steam pipes. Also, further reduction in the exterior surface temperature of the assembly can be achieved by increasing the jacket's thickness [31].

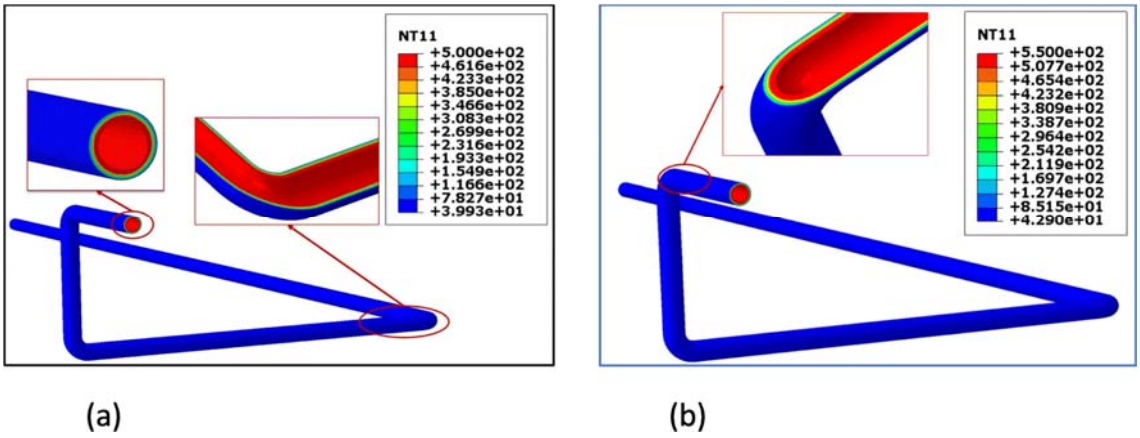

Fig. 10. Temperature distribution contour plot for **a** X20 and **b** P91 steam pipe

The creep stress and strain rate contour plot for X20 steam pipe under 1-h operational condition is shown in Fig. 11a and b, while that of P91 steam pipe is depicted in Fig. 12a and b respectively. Also shown in Fig. 13a and b is the creep stress and rate developed at the straight section of the two piping material after 1 h in service. The optimum value of creep stress developed by X20 after an hour in service is 222.1 MPa, and the creep strain rate is 3.117×10^{-5} h^{-1}, while the value of the maximum

creep stress developed by P91 after an hour in service is 220.2 MPa and the creep strain rate is 1.061×10^{-5} h^{-1}. The maximum stress and strain in both piping networks were developed on the elbow, specifically at the intrados. Thus, indicating that the intrados of the piping is the location where the pipe's failure will emanate from during service.

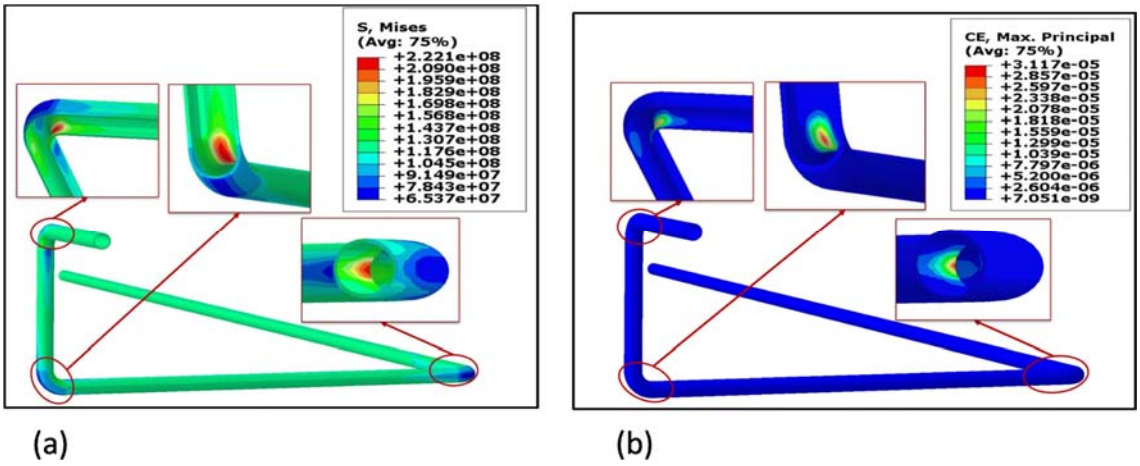

Fig. 11. Contour plot and result for X20 creep **a** stress and **b** strain rate

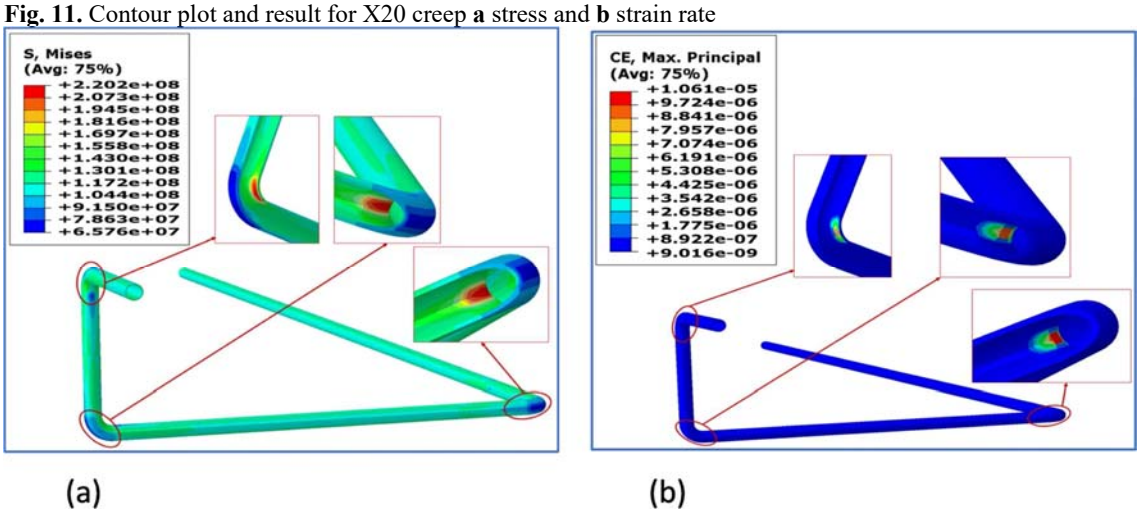

Fig. 12. Contour plot and result for P91 creep **a** stress and **b** strain rate

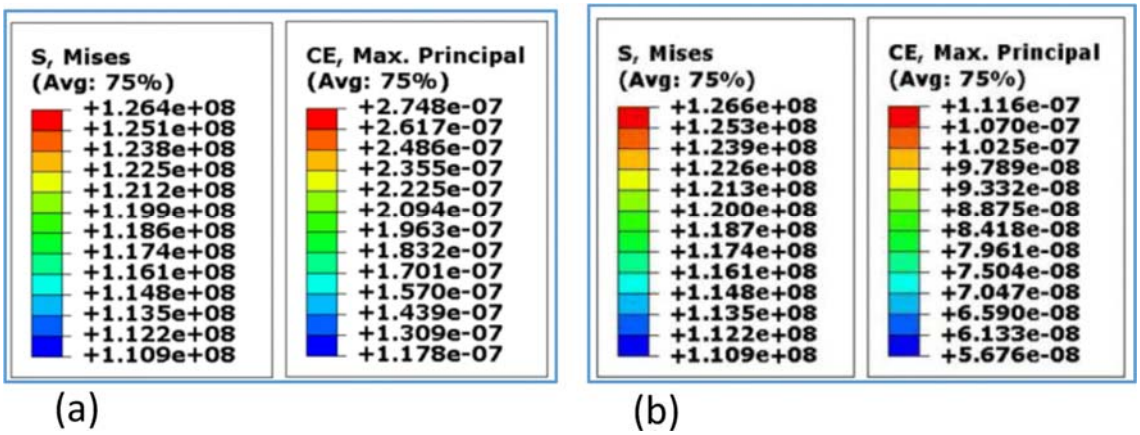

Fig. 13. Creep stress and strain rate result of straight section of **a** X20 and **b** P91 steam piping

The creep stress and strain graph plotted with respect to the operational time on a log scale for the two piping networks are shown in Fig. 14a, while the plot of the stress relaxation and the corresponding creep rate of the piping networks are depicted in Fig. 14b. In both piping networks, the creep stress decreases with an increase in time of operation, while the creep strain increases with increase in time of operation. As expected, the stress developed in both piping networks relaxes with an increase in time of operation as depicted in Fig. 14b. After an operational time of 165,195 h, the stress developed in the X20 steam pipe relaxes from 222.1 to 131.5 MPa, while the strain rate reduces from 3.117×10^{-5} to 6.67×10^{-7} h^{-1}. Similarly, the developed creep stress in the P91 steam pipe relaxes from 220.2 to 143.9 MPa, while the strain rate reduces from 1.061×10^{-5} to 3.37×10^{-7} h^{-1}. The rate of stress relaxation in X20 steam pipe was observed to be higher than that of P91, but the opposite was observed with the creep strain rate. This signifies that P91 possesses a superior creep resistance behaviour than X20 and thus will survive more useful life when both piping materials are subjected to similar service conditions.

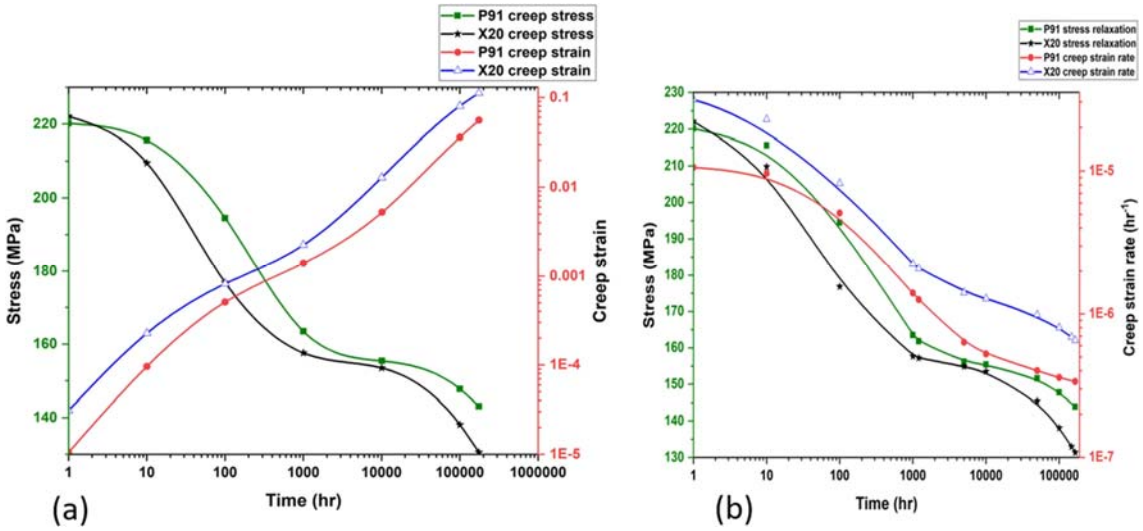

Fig. 14. a Creep stress and strain and **b** stress relaxation and corresponding creep rate of X20 and P91 steam piping as a function of time.

The obtained results and contour plots for the analysis carried out in fe-safe/Turbolife for the two different surfaces considered namely machined and fine machined-finish surfaces of the two piping networks are shown in Figs. 15 and 16. Under the specified operating temperature of 550 °C and pressure of 18 MPa, the useful creep life of the machined-finish X20 piping is 15.30 years and the creep damage is 7.479×10^{-6}, while the useful creep life of the fine machined-finish surface is 16.90 years with creep damage of 6.78×10^{-6}. Similarly, the useful creep life of the machined-finish P91 piping is 17.80 years and the creep damage is 6.414×10^{-6}, while the useful creep life and damage of the fine machined-finish surface are 18.90 years and 6.056×10^{-6} respectively. In both piping networks (X20 and P91), the worst life and creep damage were located at the elbow particularly at the intrados. Furthermore, the useful creep life of the fine machined-finish surface is higher than that of the machined finish in both piping materials. This is an indication that the useful creep life of a material is significantly influenced by the type of surface finish it was given during manufacturing.

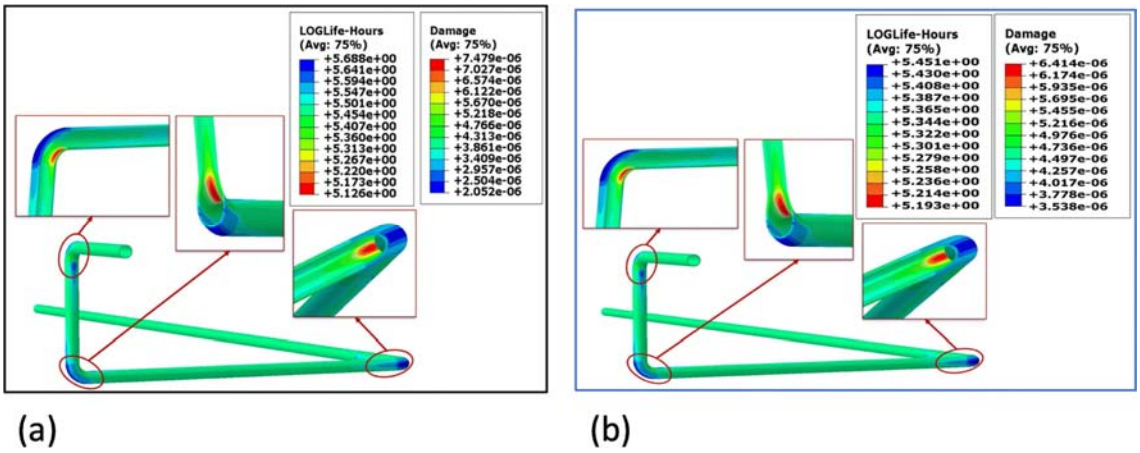

Fig. 15. Creep life and creep damage contour plots and results of **a** X20 and **b** P91 machined-finish surface steam pipe

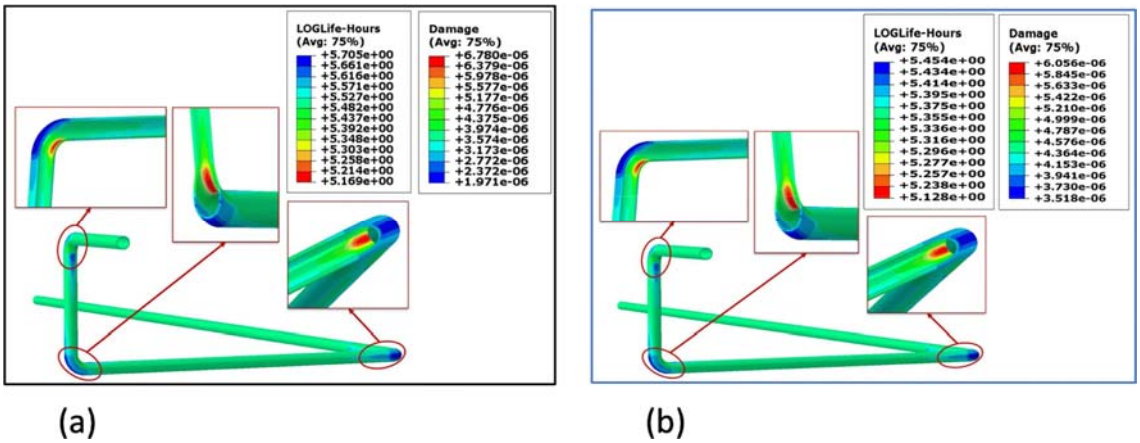

Fig. 16. Creep life and damage contour plots and results of **a** X20 and **b** P91 fine machined-finish surface steam pipe

The comparison of the useful creep life and creep damage obtained when the two piping networks were assigned machined-finish and fine machined-finish surfaces is depicted in Table 7.

Table 7 Comparison of worst/useful life and maximum creep damage of machined and fine machined-finish X20 and P91 steam piping surfaces in operation

Steam pipes	Machined finish			Fine-machined finish		
	Loglife	Life (years)	Damage ($\times 10^{-6}$)	Loglife	Life (years)	Damage ($\times 10^{-6}$)
X20	5.126	15.30	7.479	5.169	16.90	6.780
P91	5.192	17.80	6.414	5.218	18.90	6.056

Analytical validation of creep rate

Being characterized by a combination of elbows and straight pipes, the analytical validation of the developed creep rate in the piping network during service is impossible. Nevertheless, the readily available expressions for the developed mechanical and thermal stress in a straight pipe allow for the possible validation of the creep rate at the straight section of the piping network. Equations (1)–(9) are used to determine the developed mechanical, thermal, and thermo-mechanical stresses in the straight section of the piping, while the creep rate is determined using Eq. (10). Good agreement was achieved when the simulated result was compared with that obtained analytically. The simulated stress developed due to creep and the creep rate at the straight section of the piping network for the two

piping materials is shown in Fig. 13a and b, while the comparison of the numerical and analytically computed rate is shown in Table 8.

Table 8 Comparison of the analytically calculated and simulated creep rate at the straight section of the piping networks

Steam pipes	Creep rate		Deviation (%)
	Analytical ($\times 10^{-7}h^{-1}$)	Simulated ($\times 10^{-7}h^{-1}$)	
X20	2.820	2.748	2.55
P91	1.130	1.116	1.24

Conclusion

Creep failure of X20 and P91 steam piping network subjected to normal or typical power plant service condition was simulated in finite element analysis code, Abaqus CAE/2017. A Fortran creep user subroutine script written for the creep model was applied in Abaqus to determine the behaviour of the pipes during operation. Also, the damage caused by creep and the useful life of the two piping materials were computed using fe-safe/Turbolife software, and the computed creep rate, useful creep life and damage of the two piping material under the stipulated service conditions were compared. The optimum creep stress, strain and damage value were obtained at the intrados of the piping elbow in both piping materials, thus making this region of the elbow most susceptible to failure during operation. Also, the creep stress in both piping material relaxes with an increase in operational time, with X20 steam pipe having a higher stress relaxation. Nevertheless, P91 steam pipe showed a lower creep rate, creep damage and higher useful creep life when compared with X20 steam pipe. Also, the comparison of the creep rate obtained in the straight section of the two piping materials showed that there is good agreement between the simulated and calculated creep rates. Lastly, P91 steel gave a higher useful creep life than X20 steel, and thus, it is preferable for use in the fabrication of steam pipes in power generation plants.

Acknowledgement

This research has been profusely supported by Tshwane University of Technology and the University of Pretoria, South Africa. Also, the authors received relentless support of Eskom Power Plant Engineering Institute (Republic of South Africa).

References

1. Hu Z-F(2012) Heat-resistant steels, microstructure evolution and life assessment in power plants. Thermal power plants 195-226.

2. Bharasi NS, Thyagarajan K, Shaikh H, Radhika M, Balamurugan A, Venugopal S, Venugopal S, Moitra A, Kalavathy S, Chandramouli S, Tyagi AK, Dayal RK (2012) Evaluation of microstructural, mechanical properties and corrosion behavior of AISI type 316LN stainless steel and modified 9Cr-1Mo steel exposed in a dynamic bimetallic sodium loop at 798 K (525 C) for 16,000 hours. Metall Mater Trans A 43(2):561–571

3 .Bocquet P, Bourges P, Cheviet A (1993) Properties of heavy components of steel grade 91 and their welds. Nucl Eng Des 144(1):149–154

4. Sireesha M, Sundaresan S, Albert SK (2001) Microstructure and mechanical properties of weld fusion zones in modified 9Cr-1Mo steel. J Mater Eng Perform 10(3):320–330

5. Mariappan K, Shankar V, Bhaduri AK (2020) Comparative evaluation of tensile properties of simulated heat affected zones of P91 steel weld joint. Mater High Temp

6. Xu Q, Yang X, Lu Z (2017) On the development of creep damage constitutive equations: a modified hyperbolic sine law for minimum creep strain rate and stress and creep fracture criteria based on cavity area fraction along grain boundaries. Mater High Temp 34(5-6):323–332

7. Xu Q, Lu Z, Wang X (2017) Damage modelling: the current state and the latest progress on the development of creep damage constitutive equations for high Cr steels. Mater High Temp 34(3):229–237

8. Montes J, Cuevas F, Cintas J (2012) New creep law. Mater Sci Technol 28(3):377–379

9. Garofalo F (1963) An empirical relation defining the stress dependence of minimum creep rate in metals. Trans Metall Soc AIME 227(2):351–355

10. Reggiani R, Donati L, Tahar MB, Tomesani L (2018) Experimental investigation of hot-work tool steels performances under the creep-fatigue regime. Int J Adv Manuf Technol 94(5-8):1957–1967

11. Xue J, Zhou C (2016) Finite element creep damage analyses and life prediction of P91 Pipe Containing Local Wall Thinning Defect. High Temp Mater Processes 35(3):283–295

12. Tu S-T, Segle P, Gong J-M (2004) Creep damage and fracture of weldments at high temperature. Int J Press Vessel Pip 81(2):199–209

13. Hyde TH, Sun W, Williams JA (1999) Prediction of creep failure life of internally pressurised thick walled CrMoV pipes. Int J Press Vessel Pip 76(14-15):925–933

14. Hyde TH, Sun W, Williams JA (2002) Life estimation of pressurised pipe bends using steady-state creep reference rupture stresses. Int J Press Vessel Pip 79(12):799–805

15. Hall FR, Hayhurst DR (1991) Continuum damage mechanics modelling of high temperature deformation and failure in a pipe weldment. Proceedings of the Royal Society of London. Series A: mathematical and physical sciences 433(1888):383–403

16. Kachanov LK 1958 Rupture time under creep conditions.

17. Kowalewski ZL, Hayhurst DR, Dyson BF (1994) Mechanisms-based creep constitutive equations for an aluminium alloy. J Strain Anal Eng Des 29(4):309–316

18. Yang FQ, Xue H, Zhao LY and Tian J (2014) Calculations and modeling of material constants in hyperbolic-sine creep model for 316 stainless steels," vol. 457, pp. 185-190: Trans Tech Publ.

19. Annaratone D (2007) Cylinders under internal pressure. Pressure Vessel Design:47–125

20. Kanlıkama B, Abuşoğlu A, Güzelbey İH (2013) Coupled thermoelastic analysis of thick-walled pressurized cylinders. International Journal of Energy and Power Engineering 2(2):60–68

21. Kandil A, El-Kady A, El-Kafrawy A (1995) Transient thermal stress analysis of thick-walled cylinders. Int J Mech Sci 37(7):721–732

22. Pesonen V (2014) Online creep and fatigue monitoring in power plants.

23. Skelton R, Gandy D (2008) Creep–fatigue damage accumulation and interaction diagram based on metallographic interpretation of mechanisms. Mater High Temp 25(1):27–54

24. Xu L, Zhao L, Gao Z, Han Y (2017) A novel creep–fatigue interaction damage model with the stress effect to simulate the creep–fatigue crack growth behavior. Int J Mech Sci 130:143–153

25. Wen J-F, Tu S-T (2014) A multiaxial creep-damage model for creep crack growth considering cavity growth and microcrack interaction. Eng Fract Mech 123:197–210

26. Robinson EL (1952) Effect of temperature variation on the long-time rupture strength of steels. Trans ASME 77

27. Liu D, Pons DJ, Wong E (2017) Creep-integrated fatigue equation for metals. Int J Fatigue 98:167–175

28. Rasiawan T (2017) The influence of prior creep damage on the fracture localisation in X20 CrMoV12-1 cross-weld creep tests: University of Cape Town.

29. Salifu S, Desai D, Kok S (2020) Creep–fatigue interaction of P91 steam piping subjected to typical start-up and shutdown cycles. J Fail Anal Prev

30. Pyrogel-XTE-Datasheet. High-performance aerogel insulation for industrial and commercial applications.

31.Salifu S, Desai D, Kok S, Ogunbiyi O (2019) Thermo-mechanical stress simulation of unconstrained region of straight X20 steam pipe. Procedia Manufacturing 35:1330–1336

32. Salifu S, Desai D, Fameso F, Ogunbiyi O, Jeje S, Rominiyi A (2020) Thermo-mechanical analysis of bolted X20 steam pipe-flange assembly. Materials Today: Proceedings.

33. Matweb MPd. X20Cr13 Stainless steel for medical instruments 2019 [updated 2019. Available from: http://www.matweb.com/search/datasheet_print.aspx?matguid=81346c1935fc4e03bf5e1ee21d20c218

34. Salifu S, Desai D, Kok S (2020) Numerical investigation of creep-fatigue interaction of straight P91 steam pipe subjected to start-up and shutdown cycles. Materials Today: Proceedings.

35. Zhang Z, Kovacevic R (2019) A thermo-mechanical model for simulating the temperature and stress distribution during laser cladding process. Int J Adv Manuf Technol 102(1-4):457–472

36. Dassault Simulia Systemes (Providence, RI,. 2013) ABAQUS 6.13 User's manual.

37. Salifu S, Desai D, Kok S (2020) Numerical simulation and creep-life prediction of X20 steam piping. Materials Today: Proceedings.

38. Naumenko K, Altenbach H, Kutschke A (2009) A constitutive model for creep and long-term strength in advanced heat resistant steels and structures. Journal of Transition 2(3):4

39. Gorash Y, MacKenzie D (2017) On cyclic yield strength in definition of limits for characterisation of fatigue and creep behaviour. Open Engineering 7(1):126–140

40. Dassault Simulia Systemes (Providence, RI, 2017) fe-safe/TURBOlife user manual p. 12229.